

# Estimating the Number of Release Sites and Probability of Firing Within the Nerve Terminal by Statistical Analysis of Synaptic Charge

KERT VIELE,<sup>1</sup> ARNOLD J. STROMBERG,<sup>1</sup> AND ROBIN L. COOPER<sup>2\*</sup>

<sup>1</sup>Department of Statistics, University of Kentucky, Lexington, Kentucky 40506-0027

<sup>2</sup>Thomas Hunt Morgan School of Biological Sciences, University of Kentucky, Lexington, Kentucky 40506-0225

**KEY WORDS** neurotransmission; crayfish; neuromuscular junction; facilitation; quantal analysis; synapse

**ABSTRACT** Investigating the function of individual synapses is essential to understanding the mechanisms that influence the efficacy of chemical synaptic transmission. The known simplicity of the synaptic structure at the crayfish neuromuscular junction (NMJ) and its quantal nature of release allows an assessment of discrete synapses within the motor nerve terminals. Our goal in this article is to investigate the effect of the stimulation frequency on the number of active release sites ( $n$ ) and the probability of release ( $p$ ) at those active sites. Because methods based on direct counts often provide unstable joint estimates of ( $n$ ) and ( $p$ ), we base our analysis on mixture modeling. In particular, the mixture modeling approach is used to estimate ( $n$ ) and ( $p$ ) for stimulation frequencies of 1 Hz, 2 Hz, and 3 Hz. Our results indicate that as the stimulation frequency increases, new sites are recruited (thus increasing  $n$ ) and the probability of release ( $p$ ) increases. **Synapse 47:15–25, 2003.** © 2002 Wiley-Liss, Inc.

## INTRODUCTION

Recruitment of synapses is postulated to be one of the mechanisms that enhance synaptic transmission when electrical activity is increased. For example, Atwood and Wojtowicz (1999) speculate that short-term facilitation (STF) may be due, in part, to activation of previously silent synapses. Currently, various statistical measures and estimated parameters are used to quantify synaptic efficacy. Mean quantal content ( $m$ ) is commonly used as an index of the average number of single evoked events (or synaptic vesicles that fuse) that occur per stimulus, with a parameter  $n$  representing the number of sites that release a vesicle and a third parameter,  $p$ , representing the probability of an event occurring at a release site (del Castillo and Katz, 1954). Since  $n$  and  $p$  cannot be directly measured experimentally, multiple approaches have been proposed to estimate  $n$  and  $p$  using the distribution of evoked events [see reviews: Faber et al., 1998; McLachlan, 1978]. These methods work poorly when synaptic efficacy is very low, often resulting in  $n = 1$ . In these cases, the observed distribution is often fit using a Poisson distribution (Zar, 1999). However, Poisson distributions arise as an approximation for binomial distributions with large  $n$  and small  $p$ ; thus, the Poisson distribution represents the opposite extreme from  $n = 1$ .

Direct structure–function studies (Cooper et al., 1995a, 1996b) of discrete regions of motor nerve terminals have revealed that there can be many synapses (30–40), each with multiple active zones, and that the physiological measures of synaptic currents, with subsequent determination of  $n$  and  $p$ , may estimate  $n = 1$  despite quite large variations in the sizes and shapes of single evoked synaptic currents. The physiological and structural data would indicate that multiple sites are being utilized for vesicle fusion, but this is not reflected in the estimate of  $n$ .

This problem is consistent with results in the statistical literature, in particular those of Olkin et al. (1981), indicating that simultaneous estimation of  $n$  and  $p$  is inherently unstable due to the fact that the likelihood function is particularly flat as a function of  $n$ .

These results suggest that, if possible, we should search for more information in the evoked currents

Contract grant sponsor: NSF; Contract grant numbers: IBN-9808631 (to RLC), NSF-ILI-DUE 9850907 (to RLC), NSF-DMS-9971954 (to KV), and NSF-IBN-0131459 (to RLC, AJS, KV).

\*Correspondence to: Dr. Robin L. Cooper, T.H. Morgan School of Biological Sciences, 101 Morgan Building, University of Kentucky, Lexington, KY 40506-0225. E-mail: RLCOOP1@pop.uky.edu

Received 18 January 2002; Accepted 23 August 2002

DOI 10.1002/syn.10141

that may be used to estimate  $n$  and  $p$ . The sizes and shapes of single evoked synaptic currents is one such source. Using counting methods, two currents which both indicate one evoked event would be recorded identically (e.g., as one evoked event) even if the two currents appear distinctly different. Since differences in current sizes or shapes may indicate different sites firing, this may be useful information in determining the overall number of sites. The “extra information” we utilize is the area of each current trace for single evoked events. We use mixture modeling to estimate ( $n$ ) and ( $p$ ) from the area data. The area is a measure of charge (current  $\times$  time) and it is known to be less susceptible to small deviations in amplitude than the commonly used peak amplitude measures (Bekkers and Stevens, 1991; Cooper et al., 1995b).

The previous methodology involves stochastic analysis in the distribution of synaptic events measured on the postsynaptic cell (i.e., the one receiving the transmitter). An electrophysiological recording procedure, such as with a focal macropatch electrode, allows single vesicular events to be monitored directly at synaptic sites (Cooper et al., 1995b; Dudel, 1965). These events are in the form of unitary currents that represent the amount of transmitter released from a single vesicle (del Castillo and Katz, 1954). In synapses—for example, those of the crayfish neuromuscular junction (NMJ)—the activation of postsynaptic ligand gated ion channels results in a measurable postsynaptic current. Depending on the point-location within a synapse in which the vesicle fuses with the plasma membrane, the postsynaptic receptor area may only receive a portion of the transmitter. This can occur when release is by a boundary of the postsynaptic array. In theory, this may result in a different size or shape of the unitary postsynaptic current as compared to release over the center of the receptor array, but this assumes that the postsynaptic arrays of receptors are not saturated from the release of a single vesicle. On the other hand, if the postsynaptic receptor array is saturated by the release of a single vesicle, then the currents should be uniform each time that site is activated. For these two scenarios, any fluctuation in the size or shape of the postsynaptic currents observed may be either due to varied sites releasing on the presynaptic face or that various synapses are being utilized. There are examples for both cases to account for the variation in the size or shape of single vesicular events in various preparations. It is also possible that both scenarios may coexist, since one does not exclude the other from occurring. For a recent review of such issues see, Faber et al. (1998).

## MATERIALS AND METHODS

### Animals

All experiments were performed using the first walking leg of crayfish, *Procambarus clarkii*, measuring 4–6 cm in body length (Atchafalaya Biological Supply

Co., Raceland, LA). The opener muscle of the first walking legs was prepared by the standard dissection (Cooper et al., 1995a). The tissue was pinned out in a Slygard dish for viewing with a Nikon, Optiphot-2 upright fluorescent microscope using a 40 $\times$  (0.55 NA) Nikon water immersion objective. Dissected preparations were maintained in crayfish saline (modified Van Harreveld's solution: 205 mM NaCl; 5.3 mM KCl; 13.5 mM CaCl<sub>2</sub>; 2.45 mM MgCl<sub>2</sub>; 0.5 mM Hepes/NaOH, pH 7.4) at 14°C. The entire opener muscle is innervated by a single tonic excitatory motor neuron (Cooper et al., 1995a). To visualize the nerve terminals for placing the macropatch electrode over a defined region of the nerve terminal, we used the vital fluorescent dye, 4-[4-(diethylamino) styryl]-N-methylpyridinium iodide (4-Di-2-Asp; Molecular Probes, Eugene, OR), to stain the preparation. The synaptic transmission remained unaltered by this dye, as previously shown (Cooper et al., 1995a). The living preparation was stained with a 2–5  $\mu$ M dye solution for 2–5 min and then washed in crayfish saline.

### Evoked postsynaptic current (EPSC)

The EPSCs were obtained using the loose patch technique (Dudel, 1981) by lightly placing 10–15  $\mu$ m diameter, fire-polished glass electrodes directly over a varicosity. The lumen of the patch electrode was filled with the same solution as the bathing medium. The seal resistance was in the range of 100 K $\Omega$  to 1 M $\Omega$ . All events were obtained with an Axoclamp 2b (Axon Instruments, Burlingame, CA) 0.1 $\times$  LU head stage acquired at 10 kHz without additional filtering. Responses were measured and calibrated with MacLab Scope software 3.5.4 v. (ADInstruments, Grand Junction, CO). Stimulation was obtained by use of a Grass S-88 simulator and a stimulus isolation unit (Grass, SIU) with leads to a standard suction electrode (Cooper et al., 1995a).

For each of three frequencies (1 Hz, 2 Hz, 3 Hz), the excitatory axon was stimulated 1,000 times and the resulting evoked EPSCs and mEPSCs (miniature excitatory postsynaptic currents) were recorded. As shown in Figure 1, in each synaptic current recording a trigger artifact and a nerve spike can be visualized which indicates nerve stimulation. Each current recording was classified as a failure, single, or multiple event based on the observed number of peaks of discrete events in the recording. As demonstrated in Figure 1, failures and single events are discernable and can be quantified. Most of the results were failures and singles, and thus the remainder of the methodology focuses on the single events. For each single event, we measured the area (i.e., charge) under the curve for a period of time that encompasses the evoked events. The area under the curve is current-time, which is a unit of charge (Bekkers and Stevens, 1991; Cooper et al., 1995b). The area of the evoked EPSCs, the synaptic

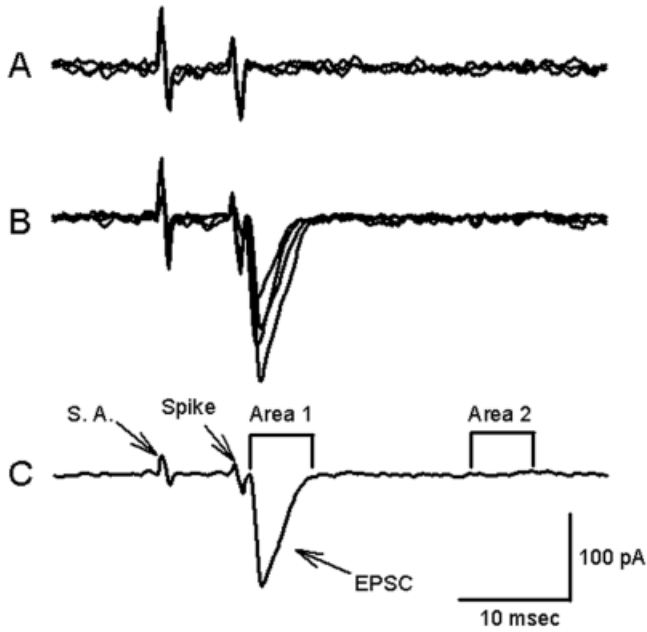


Fig. 1. Representative excitatory postsynaptic current (EPSC) traces obtained with a focal macropatch electrode placed over the nerve terminal. **A:** Three superimposed traces in which no evoked events are observed following nerve terminal depolarization. **B:** Four superimposed EPSC traces of various sizes to illustrate the range. **C:** A single EPSC represents the measures used to determine the area (i.e., charge) of the evoked currents. Area 2 is subtracted from area 1 to adjust for noise and changes in baseline throughout a recording period. The same amount of time (i.e., points) are contained in both areas. The stimulus artifact (S.A.) and the extracellular response or spike of the action potential induced in the nerve terminal are depicted by arrows.

charge, allows characterization of the postsynaptic event (Fig. 1). Measures of the charge provide an index to use over time as well as during perturbations of the stimulation frequency (Fig. 2A). In addition, the charge measures in conjunction with stochastic analysis provide the ability to determine if groupings in subtypes of single evoked EPSCs occur, which would be indicative of synaptic differences in the overall contribution to the summed EPSCs for the entire muscle. Thus, our goal is to classify the area data into distinct groups, each corresponding to an individual site.

#### Details of area calculation

The specific calculation of area consisted of identifying the duration of the EPSC from the current trace (area 1 in Fig. 1C). The baseline charge was determined by observing an area near the end of the current trace (area 2 in Fig. 1C) and computing the average voltage for that region (Southard et al., 2000). Using an average controls signal noise, while determining a separate baseline for each stimulus corrects for any DC shift that may occur over the 1,000 stimulations. In addition to the area measure, the peak amplitude was calculated for each single.

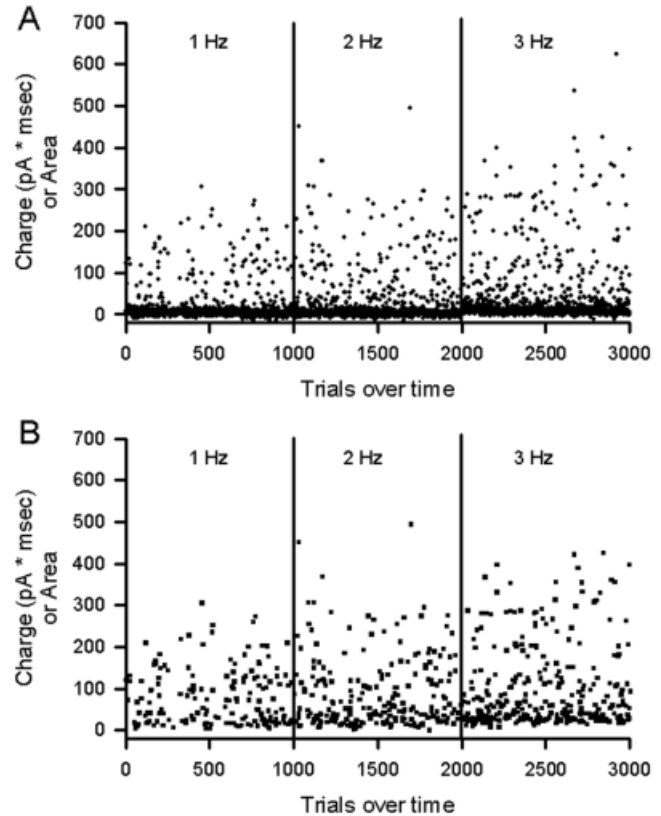


Fig. 2. The charge of the EPSCs over time for 1 Hz, 2 Hz, and 3 Hz stimulation frequencies are shown to illustrate the increased number of evoked events for the higher stimulation frequencies. The composite of all the traces, including failures to evoked EPSCs, are shown in **A**, whereas only single evoked EPSCs are shown in **B**. The failures and traces with multiple evoked releases were removed to illustrate the values used to determine subsequent analysis.

#### Square root transformation of area

The square root was taken for each value of area before performing further statistical analyses. This is a standard method for handling area data, since area is in squared units (much like using a standard deviation instead of a variance). In addition, the observed data indicated a “squaring” operation had occurred because of a large number of outliers in the untransformed area data. The square root is highly correlated with peak amplitude (correlation 0.93). Finally, as shown in “Mixture modeling” (below) a mixture of normal distributions fits the transformed data quite well.

#### Statistical methods

##### Direct count methods

A common method for obtaining the quantal parameters ( $n$ ) and ( $p$ ) is based on direct counts of the number of failures, single events, double events, etc. As mentioned above, the current traces for each of the 1,000 stimulations were classified into failures, single events, double events, and so on. Direct count methods may be used to estimate the mean quantal content (the mean number of events per stimulus, usually denoted as  $m$ ),

or they may be used to estimate ( $n$ ) and ( $p$ ) by fitting various discrete distributions such as a Poisson or some type of binomial to the count data, thus predicting the distribution of the number of events resulting from each stimulus. As one might expect, it is easier to estimate the mean of a distribution ( $m$ ) than the entire distribution. The central point of Olkin et al. (1981) is that if both  $n$  and  $p$  are unknown in a binomial distribution, then the mean  $np$  may be accurately estimated (the mean quantal content  $m$ ) but estimates of the individual parameters  $n$  and  $p$  are unstable. Olkin et al. (1981) discuss a variety of estimators in this context, such as the estimators used by Wernig (1972) to estimate  $n$  and  $p$ .

Heuristically, this instability occurs because different values of  $n$  and  $p$  produce similar predicted probabilities. For example, consider a binomial distribution with parameters  $n = 10$  and  $p = 0.2$  and a second binomial distribution with  $n = 20$  and  $p = 0.1$ . The first binomial predicts the probabilities of 0 through 5 to be 0.122, 0.270, 0.285, 0.190, 0.090, and 0.032. The second binomial predicts the probabilities of 0 through 5 to be 0.107, 0.268, 0.302, 0.201, 0.088, and 0.026. These probabilities are almost identical, even though they have different values of  $n$  and  $p$ . Note, however, they have the same value of  $np$ . Stable estimation of the mean quantal content  $m = np$  is possible, but because different values of  $n$  and  $p$  produce similar predicted probabilities, they are hard to differentiate on the basis of counts alone.

Our goal in the current research is to estimate ( $n$ ) and ( $p$ ) and thus we focus on the area data, which provides more information than the count data alone. The primary inferential technique is mixture modeling, discussed in the next section.

### Mixture modeling

We chose to model the data using a mixture of normal distributions. This model assumes that the occurrences at each particular site are normally distributed. Although the overall data may be skewed, it is possible for several overlapping normal distributions to produce skewness. This assumption of normality is explored in the Results section and appears to be acceptable in that a mixture of normals fits the data well. With this assumption, the data may be used to estimate the number of sites and the pattern of activity for a particular site (i.e., the mean, variance, and probability of the release for that site). Normal mixtures have been used before to model EPSC data, in particular in Stricker and Redman (1994) and Stricker et al. (1994). The similarities between our work and theirs are primarily methodological. We are using the same model and used the EM algorithm to find the estimates of the parameters (with the slight extension that EM algorithm was conducted with several randomly generated starting points to search for multiple modes in the likelihood

surface). While our statistical goal is similar to Stricker et al. (1994) in that we are attempting to determine the number of normal components in the mixture, the underlying data is different. Here we have attempted to isolate single quanta and are trying to group the single quanta events. In Stricker et al. (1994) the mixture components were generated by multiple sites firing simultaneously. Thus, our normal components are hypothesized to correspond to the firing distribution of a single site, with different normal components corresponding to different sites. Estimation of the number of sites  $n$  corresponds to determining the number of components in the mixture. A second, more fundamental, difference between our approach and Stricker et al. (1994) corresponds to our model selection criteria of BIC (Bayesian Information Criteria) as opposed to AIC.

Like a linear regression model, as more variables are added the fit of a mixture model is improved. Thus, we choose the appropriate number of components (sites) by examining the tradeoff between improvement in fit and the extra parameters required to add a new component to the model. We evaluated this tradeoff using BIC, where the number of components with the largest BIC is chosen as the best mixture model for the data. BIC is defined as  $\ell(\hat{\theta}) + (d/2)\ln s$ , where  $\ell(\hat{\theta})$  is the maximal value of the loglikelihood,  $d$  is the number of parameters in the model, and  $s$  is the sample size (here the number of singles). In the mixture problem,  $d = 3k-1$ , where  $k$  is the number of components (a mean, variance, and probability for each component, subject to the constraint the probabilities must sum to 1). BIC is related to AIC (used in Stricker et al., 1994) in that it is a penalized likelihood criteria. However, BIC and AIC are intended for different purposes. As discussed (with further references) in Wasserman (2000), BIC is aimed at choosing the correct model, while AIC optimizes the predictive density (sometimes called the ‘‘Akaike prediction problem’’). While the mixture problem does not obey the regularity conditions typically associated with BIC, Kerebin (1998) recently showed that BIC is still consistent (for large samples BIC will choose the correct number of components) in the mixture problem. Since our goal here is to determine the correct  $n$ , and recent results indicate that BIC performs consistently for this purpose, we have chosen to use BIC over AIC. Two review articles describing BIC, and model selection in general, are Kass and Raftery (1995) and Wasserman (2000). BIC is measured on the log scale, thus arithmetic differences are used for calibration. On the scale we used to compute BIC, a standard calibration in Kass and Raftery (1995, section 3.2) states that a difference of 0–1, 1–3, 3–5, >5 in BIC values indicates little, positive, strong and very strong evidence respectively, in favor of the model with the higher BIC value. The conclusions drawn for each of the 1 Hz, 2 Hz, and 3 Hz datasets (discussed in Results)

TABLE I. Observed distributions of failures, singles, and doubles for each of the three stimulation frequencies

	1 Hz	2 Hz	3 Hz
Events	Obs	Obs	Obs
0's	833	767	695
1's	167	229	298
2's	0	4	7
$m$	0.167	0.237	0.312

The last row provides the mean quantal content  $m$ . ' $m$ '—is the mean quantal content obtained from the direct counts [9].

all exceed this threshold for “strong evidence.” We considered models with one, two, three, and four components for each of the 1 Hz, 2 Hz, and 3 Hz datasets and found three or fewer components sufficient for each. If we had chosen the maximal number of components considered (four), we would have then considered five-component models, six-component models, and so on.

## RESULTS

### Exploratory analysis

As described above, the 1,000 trials for each dataset may be broken into three groups—failures, single evoked events, and multiple evoked events. The observed counts are shown in Table I. As can be seen, for all three stimulation frequencies most of the stimulations resulted in failures and there were very few multiple events (seven or fewer out of 1,000). There were 166 single evoked events for the 1 Hz data, 229 for the 2 Hz data, and 296 for the 3 Hz data. By themselves, these numbers indicate that either 1) individual sites fire more often at higher stimulation frequencies and/or 2) more sites are being recruited at higher stimulation frequencies. Statement (2) is actually a specific case of statement (1), since we can define “recruitment” as the probability of a site firing increasing from 0 to something greater than 0.

Our hypothesis is that the singles can be classified into distinct groups. As an exploratory first step, Figure 3 shows histograms of the Sqr(area) data for 2 Hz with two different choices of histogram breaks. Although histograms are unreliable as an inferential technique, the histograms contain multiple peaks, which indicate the data may contain distinct subgroups. The remainder of this section discusses the results of the mixture modeling that was used to infer ( $n$ ) and ( $p$ ) for each stimulation frequency.

### Mixture modeling

We performed three analyses, one for each of the 1 Hz, 2 Hz, and 3 Hz datasets. Table II and Figure 4 summarize the results for the 1-Hz data. Table II shows the BIC values and the parameter estimates, while Figure 4 shows the predicted densities for each possible number of components. The BIC shown in Table II increases substantially as the number of components is increased from one to two. This is shown graphically in Figure 4. The two-component model out-

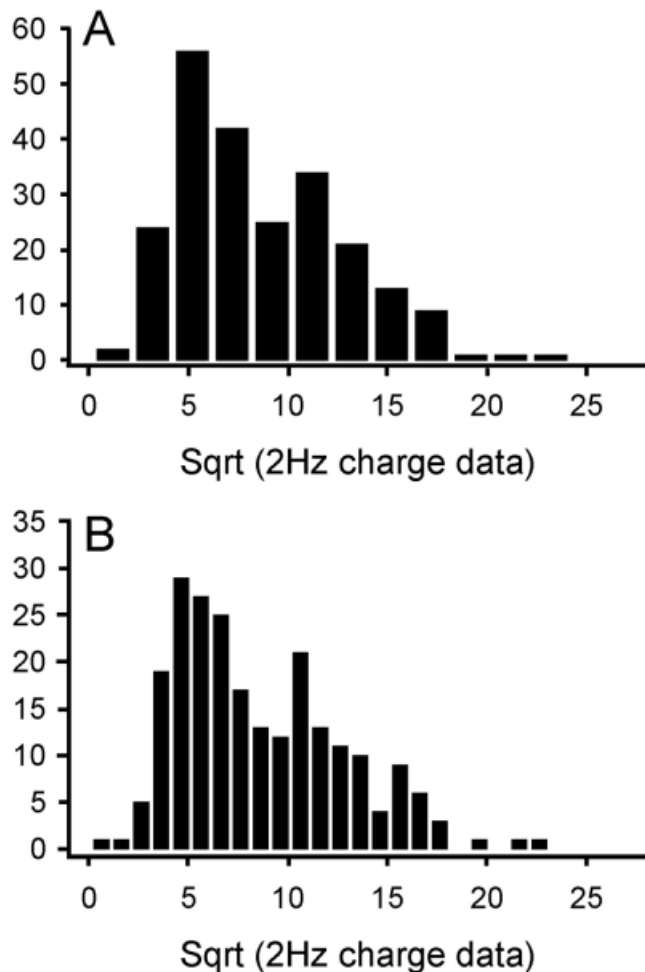


Fig. 3. **A:** Histogram for the square root of the 2 Hz charge data with breaks at 0, 2, 4, ..., 24. Visual inspection suggests that there may be modes at about 5 and 11. **B:** Histogram for the square root of the 2 Hz charge data with breaks at 0, 1, 2, ..., 24. Visual inspection suggests that there may be modes at about 5, 9, and 15.

TABLE II. Modeling of the 1 Hz charge data

# Components	BIC	Prob. of firing	Mean	Variance
1	-458.930	1.000	8.036	13.871
2	-443.552	0.433	4.599	1.500
3	-447.986	0.567	10.661	7.408
		0.364	4.223	0.922
		0.089	6.436	0.155
4	-453.633	0.547	10.833	6.800
		0.025	2.297	0.043
		0.320	4.265	0.546
		0.109	6.365	0.191
		0.547	10.837	6.780

# Components is the number of normal distributions mixed to form the model. Mean (Variance) is the mean (variance) of each of the normal distributions. BIC is the Bayesian information criteria. Prob. of firing is the probability, given that one site fires, that that particular site fires.

lines the histogram better than the one-component model. The BIC decreases when the number of components is increased to three and then to four components for this dataset. This indicates that the extra components found by the three- and four-component models

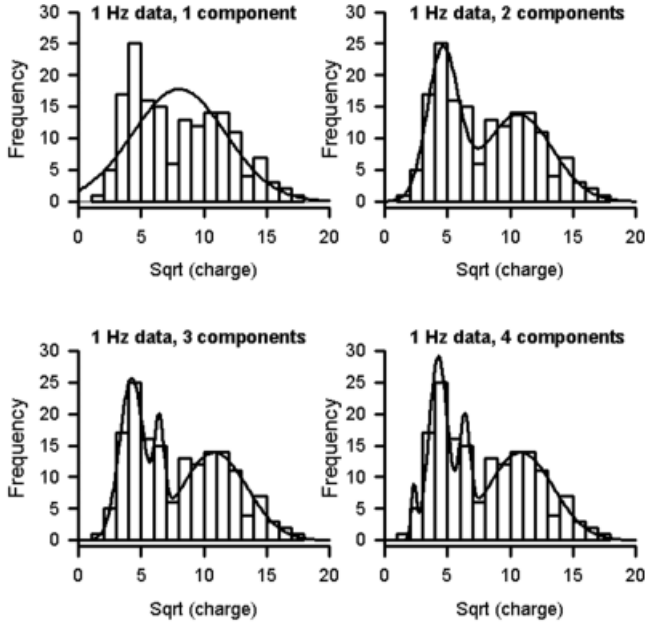


Fig. 4. Modeling the square root of the 1 Hz charge data with a mixture of normal distributions. Statistical modeling suggests that there are two modes, one centered around 4.6 and the other at about 10.7 with conditional probabilities of firing being 43%, and 57%, respectively.

are more to chance clustering of the data than due to the number of true release sites. In addition, the graphical representation of the three- and four-component models are not qualitatively better than the two-component model (Fig. 4). It appears clear that there are two modes in the one Hz data, one centered around 4.6 and the other at about 10.7.

The probabilities in the tables in this article provide the proportion of single evoked events corresponding to that site. Thus, the probabilities in Table II refer to the 166 single evoked events for the 1 Hz data. These probabilities can also be rescaled to refer to the entire 1,000 trials (failures, single evoked events, and multiple evoked events). First, we find that 43.29% of 166 trials is approximately 72 trials, which is 7.2% of the 1,000 total trials for 1 Hz. We refer to the 7.2% as the “overall” probability. Of course, it is possible that this percentage might be slightly incorrect because some of those 1,000 trials consist of multiple evoked events, which are not considered here. However, as stated in the introduction to this section, there are only a very small number of such trials in each dataset. In fact, there were none for the 1 Hz data. Thus, for the 1 Hz data the 7.2% is not subject to change by considering the multiple evoked events, and the probabilities for the 2 Hz and 3 Hz datasets described below are only subject to a slight change (less than 1%) due to the multiple evoked events not considered in this article. For the other site in the two-component estimate, the 56.71% conditional probability (proportion of single

TABLE III. Modeling of the 2 Hz charge data

# Components	BIC	Prob. of firing	Mean	Variance
1	-656.061	1.000	8.405	17.192
2	-637.393	0.434	5.104	2.099
		0.566	10.933	14.019
3	-642.985	0.203	4.022	0.508
		0.194	6.160	0.639
		0.603	10.605	15.213
4	-649.162	0.460	5.081	2.171
		0.490	10.621	9.227
		0.041	16.387	0.449
		0.0090	21.750	0.248

# Components is the number of normal distributions mixed to form the model. Mean (Variance) is the mean (variance) of each of the normal distributions. BIC is the Bayesian information criteria. Prob. of firing is the probability, given that one site fires, that that particular site fires.

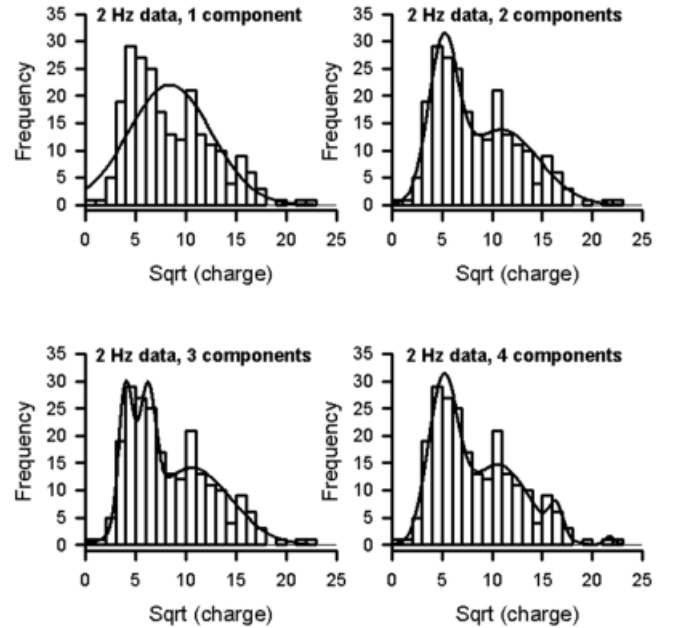


Fig. 5. Modeling the square root of the 2 Hz charge data with a mixture of normal distribution. Statistical modeling suggests that there are two modes, one centered around 5.1 and the other at about 10.9 with conditional probabilities of firing being 43%, and 57%, respectively.

evoked events) corresponds to a 9.4% overall probability.

The 2 Hz data are modeled in Table III and are depicted graphically in Figure 5. The analysis is very similar to the 1 Hz data, and again we conclude that there are two modes at about the same places. The conditional probabilities are almost exactly equal to the 1 Hz data (43.38% and 56.62%), resulting in overall probabilities of 9.97% and 13.02%. The overall probabilities are higher for the 2 Hz data because there was a larger proportion of single firings in the 2 Hz dataset. Interestingly, the variance of the second component in the two-component model is about twice the variance of the second component in the two-component model in the 1 Hz data. It is possible that a third component is present with a higher mean but not in sufficient quantity to be seen in this dataset. Table IV and Figure 6

TABLE IV. Modeling of the 3 Hz charge data

# Components	BIC	Prob. of firing	Mean	Variance
1	-863.558	1.000	8.984	19.270
2	-803.384	0.429	5.507	0.968
		0.571	11.596	17.112
3	-796.541	0.355	5.260	0.592
		0.441	8.633	5.493
		0.205	16.197	5.021
4	-800.859	0.471	5.395	0.836
		0.121	7.954	0.223
		0.179	10.348	1.179
		0.229	15.847	5.754

# Components is the number of normal distributions mixed to form the model. Mean (Variance) is the mean (variance) of each of the normal distributions. BIC is the Bayesian information criteria. Prob. of firing is the probability, given that one site fires, that that particular site fires.

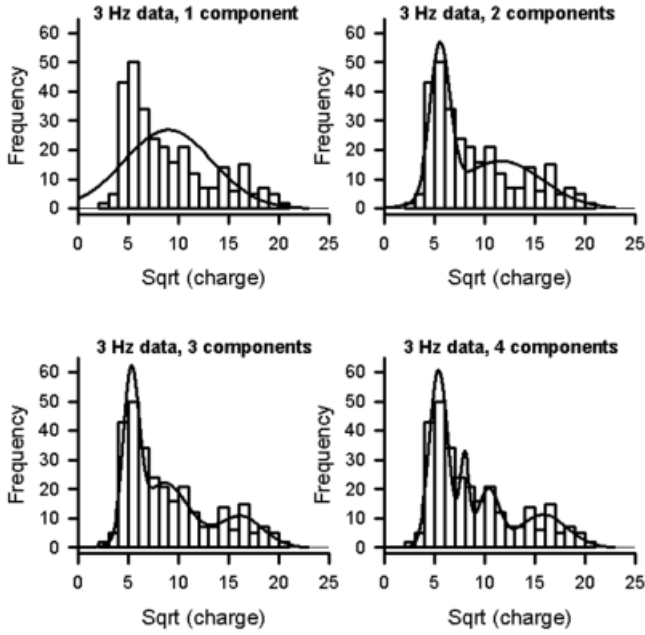


Fig. 6. Modeling the square root of the 3 Hz charge data with a mixture of normal distribution. Statistical modeling suggests that there are three modes with means at 5.3, 8.6, and 16.2 with conditional probabilities of firing being 36%, 44%, and 20%, respectively.

suggest that there are three components in the 3 Hz data with means at 5.3, 8.6, and 16.2 with conditional probabilities of firing being 36%, 44%, and 20%, respectively. The overall release probabilities are 10.58%, 13.15%, and 6.10%.

In conclusion, the data support the hypothesis that more sites are recruited as the stimulation frequency is increased, and that the probability of release is increased as the stimulation frequency is increased.

### Evaluating the fit of the normal mixture model

Of course, the mixture model assumes that the underlying components (as opposed to the entire distribution) are normally distributed, an assumption which may be controversial. To address this issue, we looked at the cumulative distribution functions predicted by the chosen models and plotted those against the em-

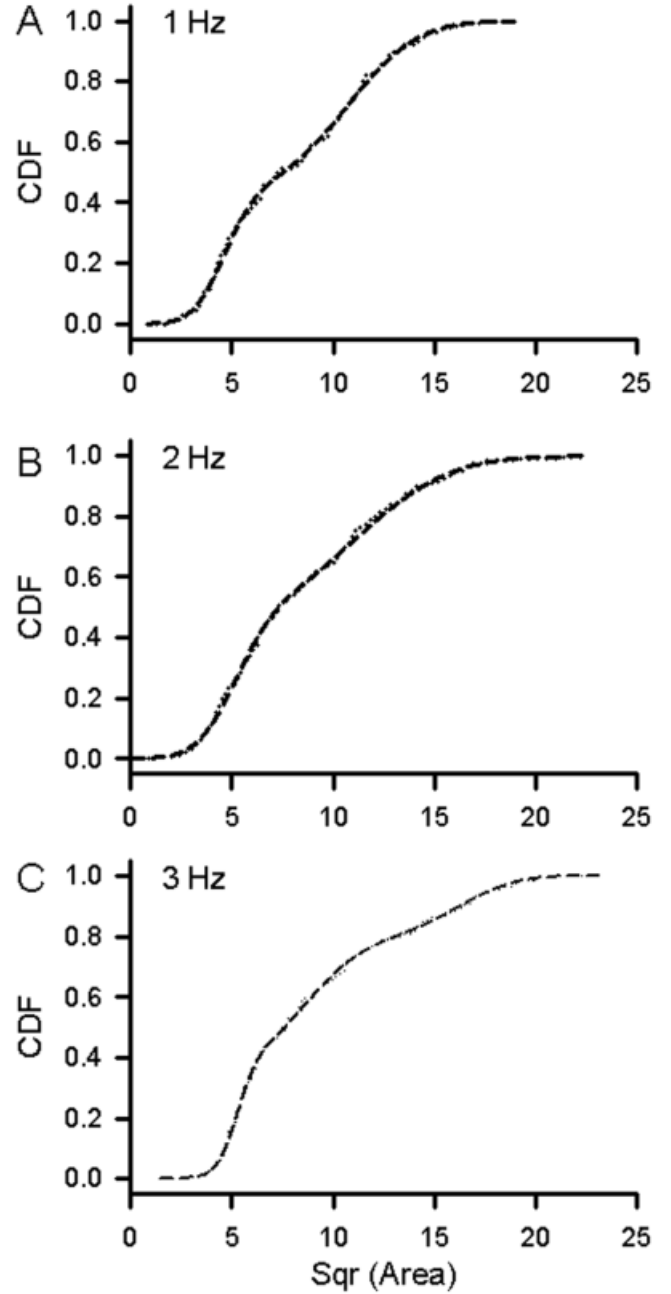


Fig. 7. Goodness of fit plots for the mixture distributions chosen by BIC. The three plots correspond to the 1 Hz (A), 2 Hz (B), and 3 Hz (C) datasets. The x-axis of each plot is the square root of the area. The y-axis provides the cumulative distribution function for each of two distributions—the empirical distribution (the observed proportion of data less than each Sqr(area) value) and the mixture distribution chosen for BIC. Thus, for the 1 Hz and 2 Hz datasets, the two-component model CDF is plotted, while for the 3 Hz dataset the three-component model CDF is plotted. The empirical CDF is a dotted line, while the mixture CDF is shown as a dashed line. Both lines are almost completely superimposed on each other for all three plots.

pirical cumulative distribution functions for each dataset. As shown in Figure 7, the fitted models fit sufficiently well that it is difficult to even observe the fitted models against the empirical CDFs. This suggests that,

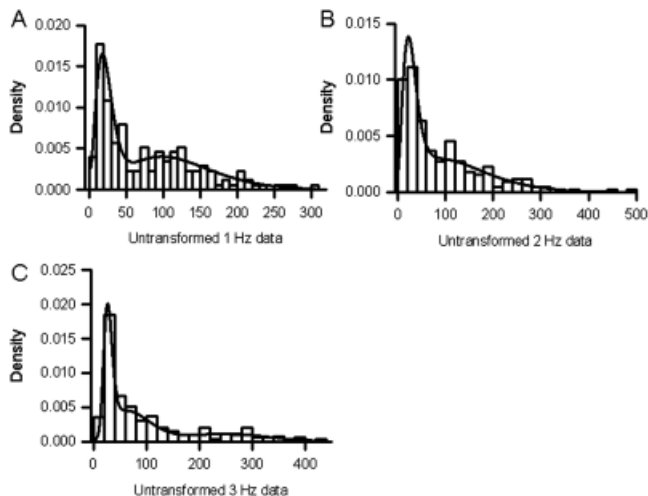


Fig. 8. Model fits for the untransformed data. These fits were computed by taking the optimal fits for each of the three datasets in Figures 4, 5, and 6, and then transforming the results back to the original (no square root) scale.

while perhaps some other model may provide an even better fit, the mixture of normal distributions does fit the data well. There may be some concern at this point that since a square root transformation was used to fit the model, the model may not be adequate on the original (no square root) scale. However, the method used in this study is analogous to a Box-Cox style transformation in regression. If one wishes, the results may be transformed back to the original scale using standard statistical results on transformations of continuous distributions. This was done in Figure 8 with the optimal fits for each of the three datasets. That is, we transformed back the two-component models for the 1 Hz and 2 Hz datasets, and the three-component model for the 3 Hz dataset. The datasets are shown on the original scale with the transformed densities. As can be seen, all three distributions have a qualitatively good fit to the original data.

## DISCUSSION

In this study we provide evidence that the classical technique (del Castillo and Katz, 1954) of directly counting the occurrences of quantal events may provide unstable estimates of the parameters  $n$  and  $p$  (see Tables I–IV). The method of direct counting overlooks the possibility that there are quantized groupings of subsets, each making up a fraction of the total percentage of quantized postsynaptic currents. This instability may be partially alleviated by looking at the current traces for extra information about  $n$  and  $p$  in the data. In particular, we focused on current trace areas and used mixture modeling to determine  $n$  and  $p$ . Of course, other measures of the current trace are possible, such as peak amplitudes or decay rates, but these alternative measures did not provide the same clarity in grouping the data as the areas did. The area data alone

strongly suggest that there at least two distinct sites firing for all stimulation frequencies, that a third site may be recruited as the stimulation is increased from 1 Hz to 3 Hz, and that the firing frequency  $p$  increases as the stimulation frequency increases.

Earlier studies investigating stimulation frequency dependence on quantal release in crayfish NMJ (Wernig, 1972) showed the same general overall trend as we report, which is that with increased stimulation frequency the number of quanta increase. However, in the Wernig study only direct counts of quantal events were taken, with use of uniform binomial statistics to estimate  $n$  and  $p$ . No attempts were made to investigate quantal populations based on the characteristics of the quantal current and, thus, what was determined as one release site most likely underestimated the number of active sites. In addition, the measurement techniques used consisted of a glass focal electrode filled with 2 M NaCl to measure synaptic current, which may well have altered the release characteristics of the nerve terminals, since it is well established that hyperosmotic solutions promote transmitter release (Quastel et al., 1971).

There is a vast amount of literature dedicated to various quantal analysis procedures and the statistical nature of synaptic transmission in a variety of systems (see reviews: Faber et al., 1998; Somogyi, 1998; Martin, 1977; McLachlan, 1978; Redman, 1997; Voronin, 1993). However, estimating  $n$  and  $p$  using the common approaches of maximum likelihood estimation (MLE) and AIC methods (Cooper et al., 1995b; Smith et al., 1991; Wojtowicz et al., 1991) do not take into account that even if only failures and single evoked events occurred there could still be multiple functional sites giving rise to the single events. This is a major limitation of the direct counting method when there are few multiple releases, as in the current data. From direct structure–function studies of varicosities, as those used in this study, it has been demonstrated that there are 30–35 synapses contained within a single varicosity and each synapse may have zero (a blank synapse), one (simple synapse), or multiple dense bodies (complex synapses) (Atwood and Cooper, 1995, 1996a,b; Cooper et al., 1995a). A dense body on a synapse is commonly referred to as an active zone since vesicles are observed to be localized around these presynaptic structures and are assumed to be released from these locations (Atwood et al., 1994; Cooper et al., 1996a; Govind et al., 1994; Propst and Ko, 1987; Walrond and Reese, 1985). However, referring to the dense bodies as active zones maybe a misnomer since they are not all likely to be active; instead, they have the potential to be active. Within these nerve terminal varicosities, which can contain 30–35 synapses, there may be in the range of 30–50 potential active zones based on the number of dense bodies observed in hundreds of serial sections (Cooper et al., 1995a, 1996b). It is known that a high

frequency of EMG activity (up to 60 Hz) occurs during the opening of the chelae in an intact animal (Crider and Cooper, 2000), and that this is likely due to a barrage of activity of the single excitatory motor neuron that innervates the opener muscle. It is practical to assume that many sites can be recruited into action during a high stimulation frequency; however, it is experimentally impractical to discern discrete quantal synaptic currents in such conditions. In addition, with a large number of multiple events within single trials it becomes impossible to directly count events to estimate  $n$  and  $p$ . Even if the counts were obtainable there is a problem in appropriately determining the best fit distributions to estimate  $n$  and  $p$  with a large number of higher ordered multiple events that may vary over time (Miyamoto, 1986). For these reasons, experimentally one makes use a low stimulation rate to observe discernable quantal events and by incrementally increasing the stimulation rate, additional release sites are able to be recruited and stochastically measured. Based on the structural analysis of these types of synapses, it is highly probable that some sites are recruited first and other sites are recruited as the stimulation frequency is increased. In fact, the structural complexity of the synapses reveal that active zones vary in their separation distances on individual synapses, which may relate to interaction of calcium domains resulting in some sites having a much higher release probability (Cooper et al., 1995a, 1996a,b). The analysis used in this study suggests that sites initially activated, which produce a given subset of quantal charges, increase in their occurrence, and that novel sites can also be recruited upon increased stimulation frequency. Studies in which vertebrate central terminals have been investigated suggest that  $n$  is positively correlated with the number of boutons (i.e., varicosities) activated (Korn et al., 1981). Most central synapses of vertebrate neurons do not have the structural simplicity of a few active zones (dense bodies) on a synapse but instead consist of a grid of dense bodies which likely will function as a unit (Vrensen, 1980). This raises the issue of what  $n$  may refer to in such cases. Is it an entire synapse or a single active zone within the grid? To the same extent, the frog NMJ has long dense bars in which multiple vesicles align themselves, and it is unknown if the entire dense bar acts as a single site (Kriebel et al., 2000). In addition, Vautrin et al. (2000) postulated that the postsynaptic responses are indirect as a result of vesicle release but directly an effect of neurotransmitter release from gangliosides on the extracellular presynaptic surface. Others (Kriebel et al., 2001) have recently postulated the existence of temporary pores different than a vesicular fusion pore to release transmitter.

The mechanisms behind quantal fluctuation of synaptic transmission can be due to postsynaptic and/or presynaptic components. A possible postsynaptic mech-

anism is nonuniform activation of the postsynaptic receptor array due to point source release of transmitter in relation to the geometry of the synapse (Bekkers, 1998; Olkin et al., 1981; Uteshev and Pennefather, 1997). In addition, the different sizes of synapses, which in some cases are related to synaptic development, account for a postsynaptic role. Saturation of the postsynaptic receptors has also been postulated to limit quantal size (Tang et al., 1994). The density and distribution of the various glutamate receptor subtypes (i.e., NMDA and AMPA) can alter the receptivity of the postsynaptic target (DiAntonio et al., 1999). When transmission is rapid from the same sites, receptor desensitization/resensitization may also contribute (Sugino et al., 2000). Presynaptic mechanisms potentially responsible for quantal fluctuation may well be due to the size differences in vesicles as well as packaging of their contents (Sulzer and Edwards, 2000; Wilson, 1998). Recently, it has also been postulated that quantal release may not be due to a single vesicle but rather to an array of vesicles releasing all at once (Kriebel et al., 2000).

Many of the proposed explanations for quantal fluctuation can be tested in "simple synapses" of the crayfish NMJ since one can monitor unitary postsynaptic currents. It is known that desensitization is not responsible for quantal fluctuation, since very low probability of release was induced, resulting in evoked events interspersed among many failures. In addition, the peak amplitudes do not show a flattened peak, which would be indicative of saturation. Resensitization is rapid in this preparation (Dudel et al., 1992). These glutamatergic ligand-gated receptors are a quisqualate type with rapid sodium conductance (Shinozake and Shibuya, 1974). There does not appear to be a wide variation in size among clear core synaptic vesicles in crayfish motor nerve terminals, but one needs to consider stereological problems in assessing vesicle dimensions (Feuerverger et al., 2000; Kim et al., 2000). Also, the size is not informative to the extent of the packaging content. With monitoring single vesicular induced EPSCs from a spatially isolated varicosity using the focal recording technique, one at least knows that the variation is not due to electrotonic spread from distant sites on the muscle, as is the problem with intracellular monitoring of the postsynaptic cell. Since the synapses are known to be of various sizes for these types of varicosities on the opener muscle (Cooper et al., 1995a, 1996b), and since "active zones" can be located at various locations on the presynaptic face, it is plausible that the geometrical differences account for the number of receptors activated. In addition, even though only a single varicosity is being monitored, there is still an issue of electrotonic spread within the subsynaptic reticulum. Since synapses occur on all regions of the varicosity and there is extensive substantial subsynaptic reticulum with massive enfoldings (Atwood and

Cooper, 1996b; Cooper et al., 1995a), this postsynaptic complexity may account for the diminution of currents monitored by the stationary extracellular recording. These pre- and postsynaptic geometric conditions then allow synapses to reliably produce a given response based on their relative location to the recording electrode. This results in some synapses giving rise to different shaped responses. Thus, it is expected to have groupings in the charge of single EPSC subsets and that new subsets may be recruited with higher frequency stimulation as well as an increase in the subsets already present. There are several reasons why charge may be more representative than peak amplitude or decay constants for release sites. If the postsynaptic receptors are saturated, then a flattening of the peak amplitude would occur. This is not a problem to measure, but the decay constant,  $\tau$ , from a truncated EPSC event would not be representative of all quantal events. In addition, the absolute peak amplitude is more subject to small changes during rapid events, and would be subjective to fluctuating more than area (i.e., charge). Thus, peak amplitude is less likely to represent the EPSC events. Alternative quantal measures, such as those put forth here, provide an avenue to better determine the number of functional release sites ( $n$ ) and the probability of release ( $p$ ).

## REFERENCES

- Atwood HL, Cooper RL. 1995. Functional and structural parallels in crustacean and *Drosophila* neuromuscular systems. *Am Zool* 35: 556–565.
- Atwood HL, Cooper RL. 1996a. Assessing ultrastructure of crustacean and insect neuromuscular junctions. *J Neurosci Methods* 69:51–58.
- Atwood HL, Cooper RL. 1996b. Synaptic diversity and differentiation: crustacean neuromuscular junctions. *Invert Neurosci* 1:291–307.
- Atwood HL, Wojtowicz JM. 1999. Silent synapses in neural plasticity: Current evidence. *Learn Mem* 6:542–571.
- Atwood HL, Cooper RL, Wojtowicz JM. 1994. Non-uniformity and plasticity of quantal release at crustacean motor nerve terminals. In: Stjärne L, Greengard P, Grillner SE, Hökfelt TGM, Ottoson DR, editors. *Advances in second messenger and phosphoprotein research. Molecular and cellular mechanisms of neurotransmitter release*. New York: Raven Press. p 363–382.
- Bekkers JM. 1998. Strontium-evoked mEPSCs reveal large quantal variance at central glutamate synapses. In: Faber DS, Korn H, Redman SJ, Thompson SM, Altman JS, editors. *Central synapses: quantal mechanisms and plasticity*. Strasbourg: Human Frontier Science Program. p 115–123.
- Bekkers JM, Stevens CF. 1991. Application of quantal analysis to the study of long-term potentiation: errors, assumptions, and precautions. In: Baudry M, Davis JL, editors. *Long-term potentiation. A debate of current issues*. Cambridge, MA: MIT Press. p 63–76.
- Cooper RL, Marin L, Atwood HL. 1995a. Synaptic differentiation of a single motor neuron: conjoint definition of transmitter release, presynaptic calcium signals, and ultrastructure. *J Neurosci* 15:4209–4222.
- Cooper RL, Stewart BS, Wojtowicz JM, Wang S, Atwood HL. 1995b. Quantal measurement and analysis methods compared for crayfish and *Drosophila* neuromuscular junctions, and rat hippocampus. *J Neurosci Methods* 61:67–78.
- Cooper RL, Harrington CC, Marin L, Atwood HL. 1996a. Quantal release at visualized terminals of a crayfish motor axon: intraterminal and regional differences. *J Comp Neurol* 375:583–600.
- Cooper RL, Winslow JL, Govind CK, Atwood HL. 1996b. Synaptic structural complexity as a factor enhancing probability of calcium-mediated transmitter release. *J Neurophysiol* 75:2451–2466.
- Crider ME, Cooper RL. 2000. Differentiation of high- and low-output nerve terminals from a single motor neuron. *J Appl Physiol* 88:987–996.
- del Castillo J, Katz B. 1954. Quantal components of the end-plate potential. *J Physiol* 124:560–573.
- DiAntonio A, Petersen SA, Heckmann M, Goodman CS. 1999. Glutamate receptor expression regulates quantal size and quantal content at the *Drosophila* neuromuscular junction. *J Neurosci* 19: 3023–3032.
- Dudel J. 1965. Potential changes in the crayfish motor nerve terminal during repetitive stimulation. *Pflügers Arch* 282:23–337.
- Dudel J. 1981. The effect of reduced calcium on quantal unit current and release at the crayfish neuromuscular junction. *Pflügers Arch* 391:35–40.
- Dudel J, Franke C, Hatt H. 1992. Rapid activation and desensitization of transmitter-liganded receptor channels by pulses of agonists. In: Narahashi T, editor. *Ion channels*, vol. 3. New York: Plenum Press. p 207–260.
- Faber DS, Korn H, Redman SJ, Thompson SM, Altman JS. 1998. *Central synapses: quantal mechanisms and plasticity*. Strasbourg: Human Frontier Science Program.
- Feuerverger A, Menzinger M, Atwood HL, Cooper RL. 2000. Assessing the dimensions of synaptic vesicles in nerve terminals. *J Neurosci Methods* 103:181–190.
- Govind CK, Pearce J, Wojtowicz JM, Atwood HL. 1994. “Strong” and “weak” synaptic differentiation in the crayfish opener muscle: structural correlates. *Synapse* 16:45–58.
- Kass R, Rafferty A. 1995. Bayes factors. *J Am Stat Assoc* 90:773–795.
- Kerebin C. 1998. Consistent estimation of the order of mixture models, technical report. Laboratoire Analyse et Probabilite, Universite d’Evry-Val d’Essonne.
- Kim S, Atwood HL, Cooper RL. 2000. What are the real sizes of synaptic vesicles in nerve terminals. *Brain Res* 877:209–217.
- Korn H, Triller A, Mallet A, Faber DS. 1981. Fluctuating responses at a central synapse:  $n$  of binomial fit predicts number of stained presynaptic boutons. *Science* 213:898–901.
- Kriebel ME, Keller B, Holsapple J, Fox GQ, Pappas GD. 2000. A new explanation for neurotransmitter secretion. *Abst Soc Neurosci* 34.2
- Kriebel ME, Keller B, Silver RB, Fox GQ, Pappas GD. 2001. Porocytosis: a new approach to synaptic function. *Brain Res Rev* 38:20–32.
- Martin AR. 1977. Junctional transmission. II. Presynaptic mechanisms. In: Brookhart JM, Mountcastle VB, editors. *Handbook of physiology. The nervous system*, vol. I. Cellular biology of neurons. Bethesda, MD: American Physiological Society. p 329–355.
- McLachlan EM. 1978. The statistics of transmitter release at chemical synapses. In: Porter R, editor. *International review of physiology. Neurophysiology III*, vol. 17. Baltimore: University Park Press p 49–117.
- Miyamoto MD. 1986. Probability of quantal transmitter release from nerve terminals: theoretical considerations in determination of spatial variation. *J Theor Biol* 123:289–304.
- Olkin I, Petkau AJ, Zidek JV. 1981. A comparison of  $n$  estimators for the binomial distribution. *J Am Stat Assoc* 76:637–642.
- Propst JW, Ko CP. 1987. Correlations between active zone ultrastructure and synaptic function studied with freeze-fracture of physiologically identified neuromuscular junctions. *J Neurosci* 7:3654–3664.
- Quastel DMJ, Hackett JT, Cooke JD. 1971. Calcium: is it required for transmitter secretion? *Science* 172:1034–1036.
- Redman S. 1990. Quantal analysis of synaptic potentials in neurons of the central nervous system. *Physiol Rev* 70:165–198.
- Richardson S, Green P. 1997. On Bayesian analysis of mixtures with an unknown number of components. *J R Stat Soc Ser B* 59:731–792.
- Shinozake H, Shibuya I. 1974. New potent excitant, quisqualate acid: effects on the crayfish neuromuscular junction. *Neuropharmacology* 13:665–672.
- Smith BR, Wojtowicz JM, Atwood HL. 1991. Maximum likelihood estimation of non-uniform transmitter release probabilities at the crayfish neuromuscular junction. *J Theor Biol* 150:457–472.
- Somogyi P. 1998. Precision and variability in the placement of pre- and post-synaptic receptors in relation to transmitter release sites. In: Faber DS, Korn H, Redman SJ, Thompson SM, Altman JS, editors. *Central synapses: quantal mechanisms and plasticity*. Strasbourg: Human Frontier Science Program. p 82–95.
- Southard RC, Haggard J, Crider ME, Whiteheart SW, Cooper RL. 2000. Influence of serotonin on the kinetics of vesicular release. *Brain Res* 871:16–28.
- Stricker C, Redman S. 1994. Statistical models of synaptic transmission evaluated using the expectation-maximization algorithm. *Biophys J* 67:656–670.
- Stricker C, Redman S, Daley D. 1994. Statistical analysis of synaptic transmission: model discrimination and confidence limits. *Biophys J* 67:532–547.

- Sugino K, Turrigiano GG, Nelson SB. 2000. Rapid scaling of AMPA quantal amplitudes in neocortical slices. *Abst Soc Neurosci* 419.12.
- Sulzer D, Edwards R. 2000. Vesicles: equal in neurotransmitter concentration but not in volume. *Neuron* 28:5–6.
- Tang C-M, Margulis M, Shi Q-Y, Fielding A. 1994. Saturation of postsynaptic glutamate receptors after quantal release of transmitter. *Neuron* 13:1385–1393.
- Uteshev VV, Pennefather PS. 1997. Analytical description of the activation of multi-state receptors by continuous neurotransmitter signals at brain synapses. *Biophys J* 72:1127–1134.
- Vautrin JY, Maric D, Sukhareva M, Schaffner AE, Barker JL. 2000. Immediately releasable transmitter store supplying quantal release at the surface of the presynaptic membrane. *Abst Soc Neurosci* 592.2.
- Voronin LL. 1993. On the quantal analysis of hippocampal long-term potentiation and related phenomena of synaptic plasticity. *Neuroscience* 56:275–304.
- Vrensens G, Cardozo JN, Muller L, van der Want J. 1980. The presynaptic grid: a new approach. *Brain Res* 184:23–40.
- Walrond JP, Reese TS. 1985. Structure of axon terminals and active zones at synapses on lizard twitch and tonic muscle fibers. *J Neurosci* 5:1118–1131.
- Wasserman L. 2000. Bayesian model selection and model averaging. *J Math Psychol* 44:92–107.
- Wernig A. 1972. Changes in statistical parameters during facilitation at the crayfish neuromuscular junction. *J Physiol* 226:751–759.
- Wilson M. 1998. The possible origin of variability in miniature PSC amplitude in cultured amacrine neurons. In: Faber DS, Korn H, Redman SJ, Thompson SM, Altman JS, editors. *Central synapses: quantal mechanisms and plasticity*. Strasbourg: Human Frontier Science Program. p 99–108.
- Wojtowicz JM, Smith BR, Atwood HL. 1991. Activity-dependent recruitment of silent synapses. *Ann NY Acad Sci* 627:169–179.
- Zar JH. 1999. *Biostatistical analysis*. Englewood Cliffs, NJ: Prentice Hall.